JOURNAL OF PROPULSION AND POWER
Vol. 24, No. 1, January–February 2008

Plume Expansion and Ionization in a Microlaser Plasma Thruster

Michael P. Reilly* and George H. Miley†
University of Illinois at Urbana–Champaign, Urbana, Illinois 61801
and
William A. Hargus Jr.‡
U.S. Air Force Research Laboratory, Edwards Air Force Base, California 93524

DOI: 10.2514/1.23512

Ion density measurements have been performed on the plasma generated by an ablative diode laser thruster using a negatively biased flat plate probe. The biased probe data were coupled with measurement of the ablation crater through use of a scanning electron microscope. The scanning electron microscope was used to analyze the postpulse ablation spots to determine the volume of fuel ablated. The microlaser plasma thruster discussed here ablates a target material through the backsurface by focusing the laser through a transparent substrate in a process typically referred to as transmissive mode ablation. The target materials investigated were polyvinyl chloride and glycidyl azide polymer, while the substrates used were cellulose acetate and Kapton®. Peak ion densities for a glycidyl azide polymer (target)/acetate (substrate) were found to be 1.6×10^7 cm^{-3}, whereas for glycidyl azide polymer/Kapton and polyvinyl chloride/acetate the peak ion densities were 4.5×10^7 and 7.9×10^9 cm^{-3}, respectively. Although these corresponded to low ionization fractions calculated from the observed mass loss, the results indicate there are ways to improve the ionization fraction and in turn increase the specific impulse.

Nomenclature

A_c	=	area of current flow, cm^2
d_{fuel}	=	depth of abated fuel spot, cm
f_{IONS}	=	ionization fraction
I	=	total ion current, A
I_{sp}	=	specific impulse, s
MW_{fuel}	=	molecular weight of fuel, g/mol
m_{fuel}	=	mass of fuel, g
N_A	=	Avogadro's number
$\bar{N}_{\text{fuel}}$	=	average number of particles per ablation shot, cm^{-3}
$\bar{N}_{\text{ion}}$	=	average number of ions per ablation shot, cm^{-3}
$\bar{n}_{\text{ion}}$	=	average ion density, cm^{-3}
n_{molecule}	=	number of molecules per polymer
q	=	charge, C
r_{fuel}	=	radius of fuel ablation spot, cm
V_c	=	volume of charged particles, cm^3
V_{fuel}	=	volume of ablated fuel, cm^3
v_{ion}	=	average ion velocity, cm/s
Δt	=	time step, s
Δx	=	average length of fully developed plume, cm
ρ_{fuel}	=	density of fuel, g/cm^3
ϕ_c	=	diameter of discolored region on probe, cm

Presented as Paper 4072 at the 41st AIAA/ASME/SAE/ASEE Joint Propulsion Conference & Exhibit, Tucson, Arizona, 10–13 July 2005; received 27 February 2006; revision received 7 March 2007; accepted for publication 9 June 2007.

*Graduate Student, Department of Nuclear, Plasma, and Radiological Engineering, 103 South Goodwin MC-234. Student Member AIAA.
†Professor, Department of Nuclear, Plasma, and Radiological Engineering, 103 South Goodwin MC-234. Senior Member AIAA.
‡Research Engineer, 10 East Saturn Boulevard. Senior Member AIAA.

I. Introduction

LASERS are essential in such applications as data storage, energy production through fusion, materials strengthening and fabrication, and communications. They are also increasingly vital as industrial companies researching extreme ultraviolet light for next generation lithography transition to a laser-based source. The understanding of laser-material interactions is of fundamental significance to enabling these technologies.

An additional application of lasers is that of a laser-based microthruster for satellite propulsion [1,2]. Possible uses include primary propulsion of very small satellites as well as very precise attitude control for larger satellites. With the increasing availability and efficiencies of diode-based lasers, laser ablation of select materials provides a possible mechanism to produce microelectric thrusters [1]. The use of a microlaser plasma thruster (μLPT) will allow for progress toward the development of nano- and picosatellites, by allowing for an overall weight reduction due to the small size of this propulsion unit. An understanding of the ablation physics and plasma properties in the plume could lead to methods to achieve higher values of specific impulse (I_{sp}) and thrust.

There are two methodologies in which laser ablation produces useful thrust. In both cases, the plume of ablated material exhibits a $\cos^n(\theta)$ distribution with n varying between 2.5 and 30 [3–5]. The first case is the reflective, or R mode, illustrated in Fig. 1, where the laser is incident on the front surface of the target mass. The laser heats the surface, boiling off material. This vapor phase material is then further heated by the incident flux. If the laser pulse is sufficiently intense, the heating produces a one-dimensional planar expansion. This results in a nearly lossless thermal expansion. However, the R mode is limited due to the coating of laser optics by the ablated materials. An alternative is to use the transmissive or T-mode geometry also illustrated in Fig. 1. In this variation, the incident laser flux passes through a transmissive layer (substrate) to the ablatant.

In the R-mode geometry a greater exhaust momentum and I_{sp} are achieved than the T mode [2]. This is due to a layered ablation effect. In R mode, the incident flux initially heats the outermost layer allowing for more laser energy to ionize the expanding material through absorption. A greater number of ionized particles will generate higher values of I_{sp}. In contrast to R mode, the incident flux in T mode must heat all absorbing target material below the outermost layer before allowing the remaining energy to be directed

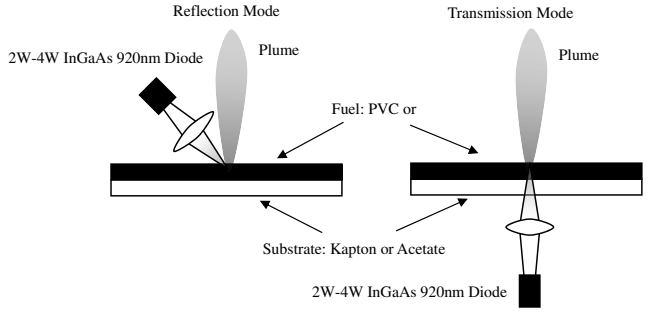

Fig. 1 Transmissive mode (T-mode) ablation vs reflective mode (R-mode) ablation.

toward ionizing the expanding material. This results in a lower exhaust momentum and lower I_{sp}. In fact, considering the extreme T-mode scenario where the target material is too thick, all of the incident flux would be directed toward heating and possibly no ejection of material would occur. A much greater in-depth evaluation of the performance characteristics that separate R-mode and T-mode ablation is described by Phipps [1,2]. Additionally, extensive modeling of the T-mode ablation has been conducted by Keidar and Boyd [6,7], although power densities considered in their work are much greater than those used in this study.

Regardless, it is favorable to keep the deposited energy near the laser focus spot. This reduces radial heating losses within the target. Therefore, materials with low thermal conductivities are considered especially for diode lasers with relatively low fluences. Specifically in this study, organic polymers are used as ablation targets in contrast to using metals. Not only does the low thermal conductivity of organic polymers reduce radial heating losses but it also relaxes the power requirement of the laser. However, the use of a low-voltage diode laser requires a longer pulse length to achieve the necessary fluence in order to initiate ablation. In this study, the laser fluence used is $\sim$5 kJ/cm^2.

II. Experimental Setup and Apparatus

A. Vacuum System

Testing was conducted in a 50-cm diam by 1-m long cylindrical vacuum chamber. The chamber is pumped by a Varian V-300 turbomolecular vacuum pump with a pumping speed of 250 l/s backed by a dry scroll pump. Chamber pressure during testing is maintained in the 10^{-6} torr range as measured with a Varian cold cathode ionization gauge calibrated for nitrogen (air). The vacuum chamber is mounted on a $120 \times 300 \times 30$ cm optics table. Both the table and turbomolecular vacuum pump are vibrationally isolated by pneumatic legs and a damping elastomer flange, respectively.

B. Single Shot μLPT

The μLPT apparatus used in these experiments employs a single shot prototype supplied by Photonics Associates. It uses a commercial 920-nm wavelength, InGaAs low-voltage diode laser (JDS-UniPhase; Model SDL 6380-A). Although the laser power is low for ablation ($\sim$4 W), the tight focus of the beam yields high power densities (250 kW/cm^2).

The single shot μLPT used in this study was specifically constructed for plume diagnostics. A flight model μLPT would have a mechanism to provide a greater propellant throughput. However, the essential physics governing the ablation are identical. In the case of the single shot μLPT, the fuel is hard mounted to the front of the device. Hard mounted is defined as the fuel/substrate secured to the front of the device with Kapton tape as shown in the schematic in Fig. 2 and in the photograph shown in Fig. 3. In this case, it is the aluminum mount, with the fuel/substrate tape, that rasters across the stationary diode laser. It is in this T-mode geometry where the laser is mounted behind the target/substrate material.

The single shot μLPT shown in Fig. 3 has precision control of each ablation shot so that a diagnostic can be performed on each ablation

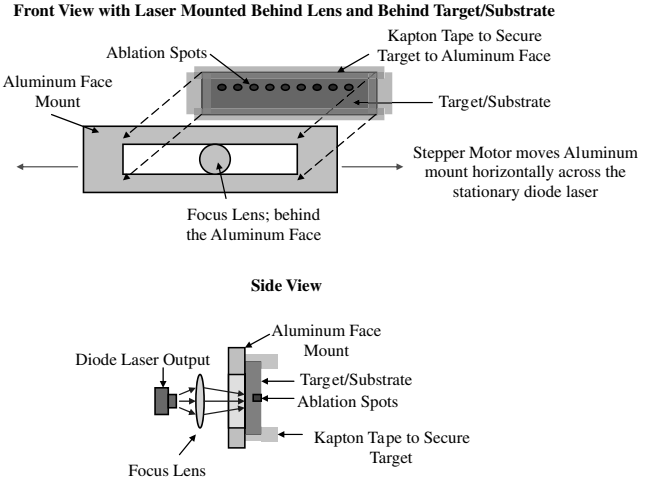

Fig. 2 Mounting of target/substrate.

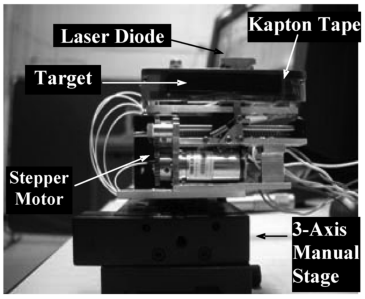

Fig. 3 Front view of μLPT with target/substrate mount.

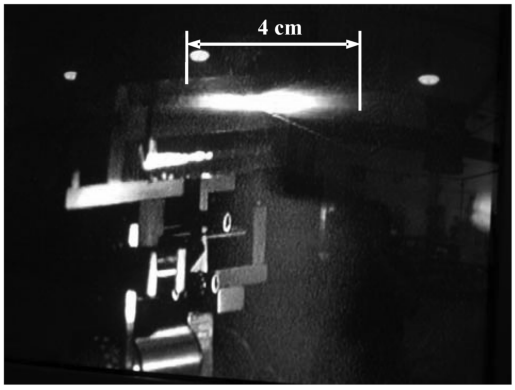

Fig. 4 Photo of first 3 ms of μLPT discharge.

event. In Fig. 3 the diode laser is transmitted from the rear of the target and particulate is ejected out of the page. The movement of the target material is performed by a LabVIEW program controlling a microstepper motor which horizontally traverses the target/substrate. This microstepper uses an integral 76:1 step-down gearbox acting through a 16:15 reduction gear. This allows for approximately 56,400 steps for 5 cm of travel, corresponding to a control of about 1 μm. This control is ideal considering the μLPT's ablation spots are about 120 ± 20 μm in diameter.

Figure 4 shows the μLPT in operation. This photograph of the plume was taken during the first half of the discharge. It visually measures about 4 cm in length. Pictures taken with a high-speed camera show that on average the plume expands from the fuel face to this length during the first millisecond. Although this is typically what occurs, high-speed photographs show that occasionally a smaller plume was evident. The variation in plume expansion during the first millisecond is shown in Fig. 5.

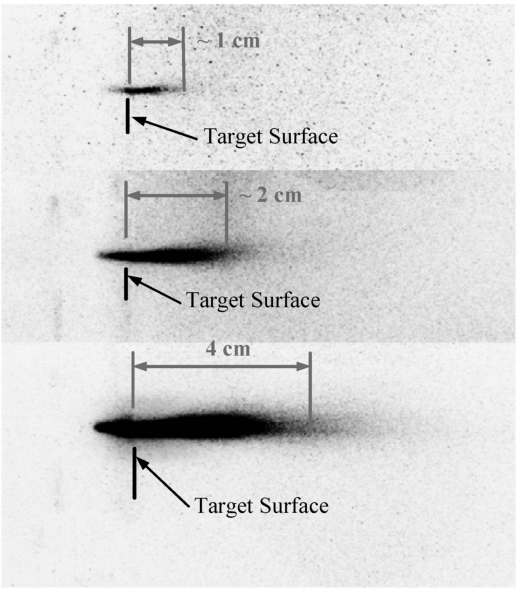

Fig. 5 Plume expansion from target surface.

All three ablation events are the result of the same amount of laser energy being deposited: 24.5 mJ over 5 ms. These photographs do not indicate any relative degree of ionization between each event; however, the same amount of energy is deposited each time and therefore the difference in plume lengths is attributed to the thickness variations along the fuel surface. The plume expansion at the top of Fig. 5 is due to a smaller thickness of fuel being ablated than the other two expansions shown. As mentioned previously, the average length of the plume expansion during the first millisecond was observed to be 4 cm (bottom plume of Fig. 5). High-speed photographs at later times of plume expansion were not observed because the setup required a second delayed trigger which was not employed at the time.

C. Ion Current Collection Probe

The negatively biased flat plate probe consists of a 15-cm diam copper plate biased to −9 V. This bias was expected to be sufficient due to the moderate power densities of hundreds of kW/cm^2. At these power densities, the degree of ionization was expected to be low: $\ll 1$ (for comparison, above power densities of 5 GW/cm^2, the ionization fraction approaches unity) [8]. As a consequence, the electron and ion energies were expected to be sufficiently below this value such that the probe was saturated by the ion current. This bias was performed using a dry cell battery. This bias technique is preferred to a dc power supply due to the significant reduction in noise. It is assumed that the secondary electron emission from the low-energy incident ions and neutrals is negligible [9]. Ion current measurements were performed by monitoring the voltage drop across a 200 kΩ resistor. A schematic of the probe is shown in Fig. 6a and a photograph in Fig. 6b.

There is a visible discoloration on the copper probe in Fig. 6b due to the deposits of propellant particulates from a 150 shot series of μLPT firings. The arrows in Fig. 6b denote the extent of the discoloration/deposits. It should be noted that in Fig. 6b, some of the nonuniform appearance of the copper is due to its surface finish and is not the result of the incident plume. The diameter of the plume was taken from visual inspection of the width of the deposits on the probe. These were measured at each downstream location to determine the approximate diameter of the plume.

D. Target Material and Substrate

The combinations of target/substrate considered were a 60-μm thick fuel strip of polyvinyl chloride (PVC) layered on top of a 100-μm thick substrate of cellulose acetate and a 300-μm thick fuel strip of glycidyl azide polymer (GAP) layered on top of a 60-μm thick substrate of cellulose acetate or Kapton. The target/substrate thickness was determined from a scanning electron microscope (SEM) measurement. Some of the physical characteristics[§] [10] for these materials are listed in Table 1.

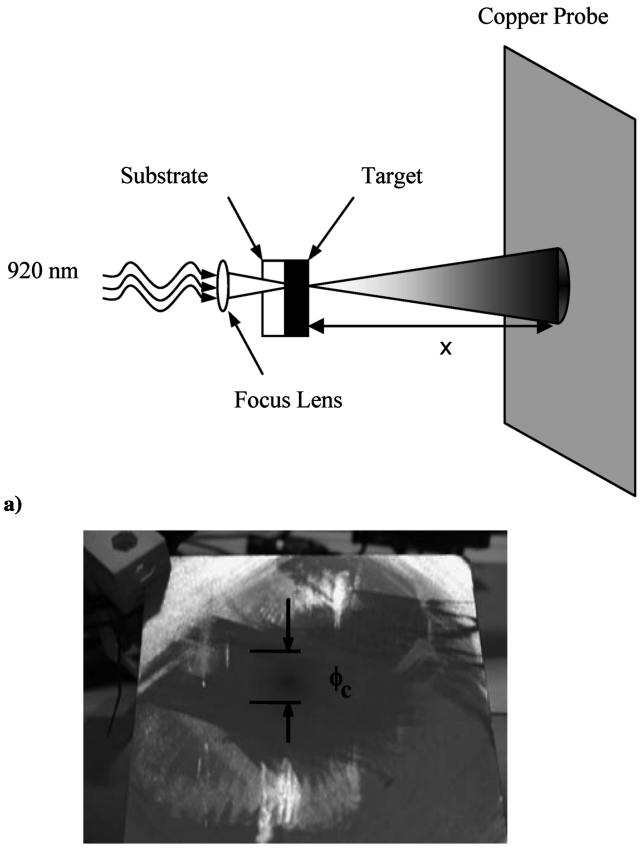

Fig. 6 a) μLPT mode with copper probe; b) actual probe used for ion current measurement.

III. Calculations

A. Average Ion Density

Taking an average over the target-to-probe distance and over the discharge time, the average ion density $\bar{n}_{\text{ion}}$ in the plume can be obtained through a measurement of the probe current using the relation [11]

$$I = \bar{n}_{\text{ion}} q v_{\text{ion}} A_c; \qquad \bar{n}_{\text{ion}} = \frac{I}{q v_{\text{ion}} A_c} \tag{1}$$

In this expression, I is the total current collected on the biased probe and a singly ionized plasma was assumed, so $q = 1$. To ensure that the total current was measured, the probe was made much larger than the plume. The area of current flow A_c was approximated from the probe discoloration discussed earlier relative to Fig. 6b. The ion velocity v_{ion} can be written as

$$v_{\text{ion}} = \frac{\mathrm{d}x}{\mathrm{d}t} \cong \frac{\Delta x}{\Delta t} \tag{2}$$

where Δx is the distance from the target face to the probe and Δt is the time step (length of the laser pulse) such that $I\Delta t$ is the total charge collected by the probe. The average ion density can then be calculated by assuming an average ion velocity over the 5 ms (Δt)

[§]"Material Safety Data Sheet; MSDS," http://www.msds.com [cited 30 November 2001]. And, also see Dupont, "Material Safety Data Sheet; MSDS," http://www.dupont.com/kapton/index.html [cited 01 June 2005].

Table 1 Physical characteristics of target materials and substrates. Note: the indices of refraction listed for the substrate materials are those for the sodium D line at 589.3 nm

Target	Chemical formula	Density
Glycidyl azide polymer	$C_3H_5ON_3$	1.29 g/cm^3
Polyvinyl chloride	CH_2CHCl	1.35 g/cm^3
Substrate	**Index of refraction**	**Density**
Acetate	1.48	1.22 g/cm^3
Kapton	1.70	1.42 g/cm^3

discharge of the μLPT. Then substituting Eq. (2) into Eq. (1), the averaged ion density becomes

$$\bar{n}_{\text{ion}} = \frac{I\Delta t}{A_c \Delta x} \tag{3}$$

Then taking V_c as the volume of charged particles found from approximating the plume as a cone with the base ϕ_c determined by the discoloration of repetitively firing the device at the probe as shown in Fig. 6b

$$V_c = A_c \Delta x \tag{4}$$

where ϕ_c and Δx were also used to calculated the plume angle of expansion illustrated in Fig. 7

$$\theta = \tan^{-1}\left(\frac{\phi_c}{2\Delta x}\right) \tag{5}$$

Typically, the half-angle of the plume expansion is approximately 19 deg. Finally, substituting the calculated volume expression (4) into Eq. (3) gives an expression for the average ion density as

$$\bar{n}_{\text{ion}} = \frac{I\Delta t}{V_c} \tag{6}$$

This relation is the result of averaging over the discharge time as well as averaging over the spatial distance from the fuel surface to the probe.

B. Ionization Fraction

In addition to calculating the average ion density of the plume, the ionization fraction can be approximately calculated using the average number of particles ejected per shot with the average ion density measurement:

$$f_{\text{ions}} = \frac{\bar{N}_{\text{ion}}}{\bar{N}_{\text{fuel}}} \tag{7}$$

where the bar indicates an average over time and space. The average number of ions per ablation shot was taken as

$$\bar{N}_{\text{ion}} = \bar{n}_{\text{ion}} V_{\text{fuel}} \tag{8}$$

V_{fuel} is the volume of the ablated fuel illustrated in Fig. 8a with a corresponding SEM photo shown in Fig. 8b. The area of the fuel A_{fuel} and the depth of the fuel d_{fuel} are taken from the SEM photo of Fig. 8b.

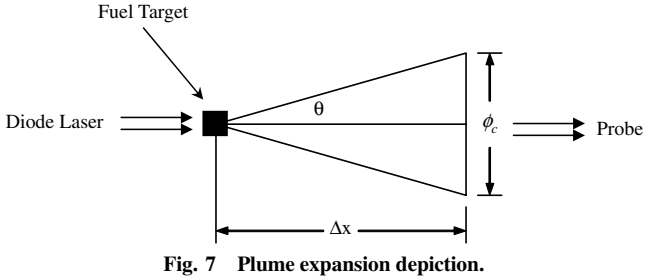

Fig. 7 Plume expansion depiction.

Using the following definitions:

$$A_{\text{fuel}} = \pi r_{\text{fuel}}^2 \tag{9}$$

$$V_{\text{fuel}} = A_{\text{fuel}} d_{\text{fuel}} \tag{10}$$

$$m_{\text{fuel}} = V_{\text{fuel}} \rho_{\text{fuel}} \tag{11}$$

the number of total particles per ablation shot was calculated from

$$\bar{N}_{\text{fuel}} = \frac{m_{\text{fuel}} N_A}{MW_{\text{fuel}}} n_{\text{molecule}} \tag{12}$$

In this expression, the total number of particles per ablation shot is defined as

$$\overline{N}_{\text{fuel}} = \frac{(\text{mass loss in g})(\text{no. molecules/mol})}{(\text{g/mol})} (\text{particles/molecule}) \tag{13}$$

here n_{molecule} is the number per molecule in PVC or GAP. This value is necessary to calculate the ionization fraction f_{ions} or the total number of ions created to the total number of atoms ejected.

IV. Results

A. GAP/Acetate

The first target/substrate that will be discussed is the GAP/acetate. SEM analysis (Figs. 9a and 9b) shows that the ablation spot diameter on the GAP is 130 $\pm$ 10 μm. These spot sizes are for when the laser deposited 24.5 mJ over 5 ms. The depth of the ablation spots is 300 μm, which is the full thickness of the GAP as shown in Figs. 9a and 9b. The substrate thickness is 60 μm and there is little to no visible burning of the substrate by laser ablation when viewing SEM results. It should be noted that there is expected to be some laser energy loss due to attenuation from the different indices of refraction for each substrate (Table 1) [12].

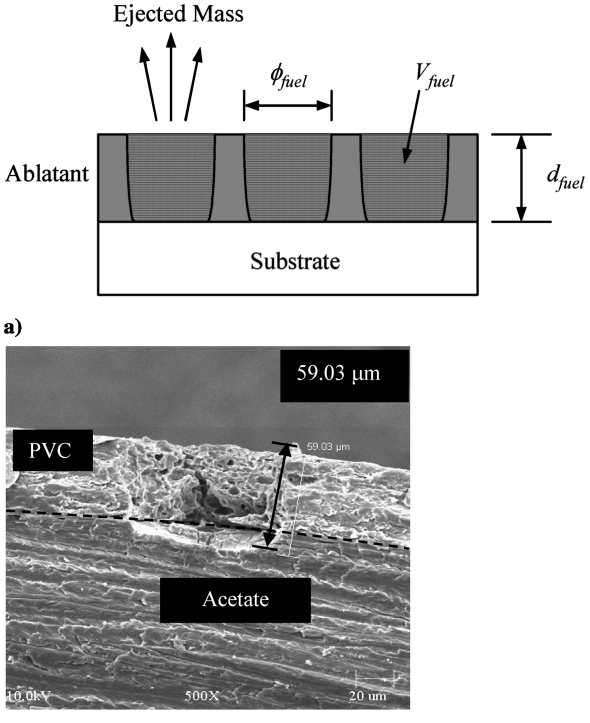

Fig. 8 a) 2-D schematic of volumetric fuel ablated; b) SEM photo of the PVC/acetate ablation spot.

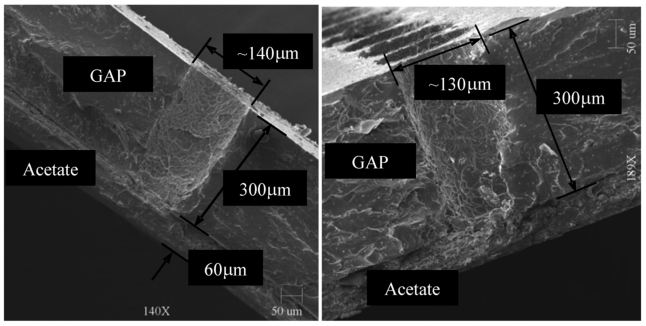

a) b)

Fig. 9 a) GAP/acetate SEM photo; b) GAP/acetate SEM.

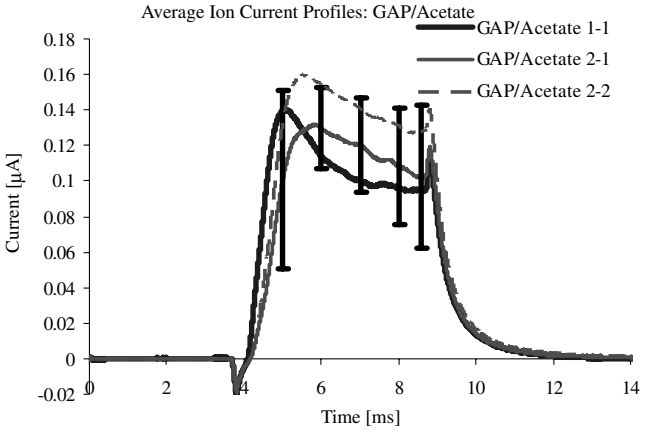

Fig. 10 GAP/acetate average ion currents.

The average volume of the GAP ablated measured from SEM results was 4.0×10^{-6} cm^3. This corresponded to an average of 5.1×10^{-6} g/shot or 5.1 μg/shot of ejected GAP. This calculation was simply based on the material density of the GAP from Table 1.

The average ion current profiles for 150 successive shots on the same fuel strip over the 5 ms discharge are shown in Fig. 10. Error bars were determined as the standard deviation of 150 individual current profiles. The dip at the start of the discharge and the spike at the end of the discharge are electrical noise from the laser switching on/off. Each of the three profiles seen here are the result of averaging over 150 sequentially pulsed discharges on the same fuel strip. The figure indicates that using two different fuel strips of GAP/acetate, a similar performance is reached. This is evident in the similar magnitudes in the peak ion currents between fuel strip 1 and fuel strip 2. The peak currents are between 130–160 nA. Interest was given to the downstream location where the ion current reaches a maximum. This location was found to be about 7 cm downstream of the target face. The average ion density 7 cm from the target face was 1.6×10^7 cm^{-3}. This corresponded to an ionization fraction of 9.8×10^{-9} found from the ratio of the number of ions to the total number of particles ejected [Eq. (7)].

The variation in peak ion currents across each fuel strip is shown in Fig. 11. The distance that these 150 ablation shots cover on the fuel strip is 2.5 cm. Over this distance the peak ion current experiences highs and lows which are assumed to be due to local fuel thickness variations.

B. GAP/Kapton

The same target material GAP is again studied, but with a Kapton substrate in contrast to acetate. SEM analysis shows the fuel thickness of the GAP is 100 μm while the Kapton is 160 μm thick (Fig. 12). The fuel thickness of the GAP/Kapton is not as thick as the previous GAP/acetate (300 μm GAP/acetate versus 100 μm GAP/Kapton, Figs. 9a and 9b). The ablation crater diameters again are 130 ± 10 μm as shown in Fig. 12. These are similar to the GAP/

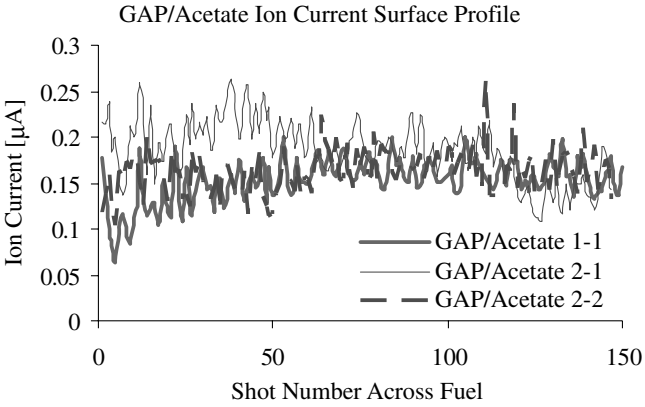

Fig. 11 GAP/acetate average ion currents.

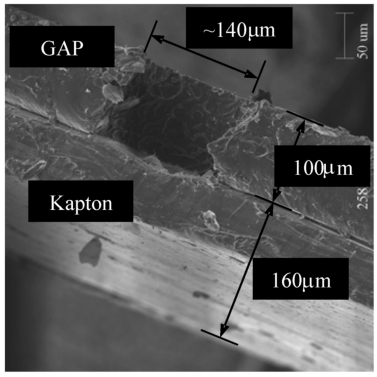

Fig. 12 GAP/Kapton SEM photo.

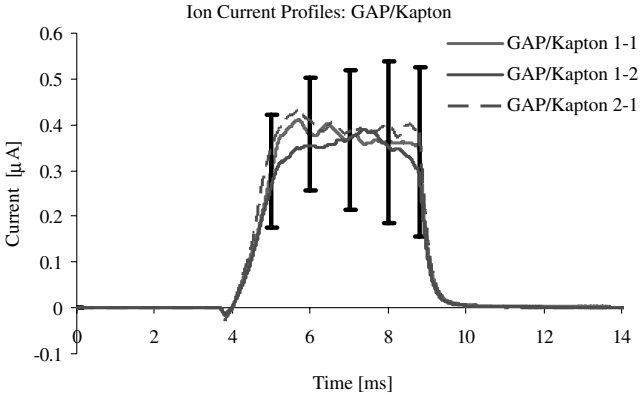

Fig. 13 GAP/Kapton average ion currents.

acetate case, although now because of the difference in thickness of the GAP, the average volume of mass ablated is 1.3×10^{-6} cm^3. This total volume of mass ablated is lower than when the GAP was backed with acetate. The amount of GAP mass ejected is calculated to be 1.7 μg/shot, a 33% reduction when compared with GAP/acetate.

The average ion current profiles are shown in Fig. 13. The peak ion currents are between 600 nA and 1 μA. This is significantly higher than when the GAP was backed with acetate. However, this result should be expected. In this case, the GAP thickness was reduced by a factor of 3 and less total mass was ejected, but approximately the same amount of laser energy was deposited. With more laser energy now available for ionization instead of heating and neutral particle ejection, a higher ionization level is expected.

The downstream location where the ion current peaks is again 7 cm from the target face. The average ion density measured here is

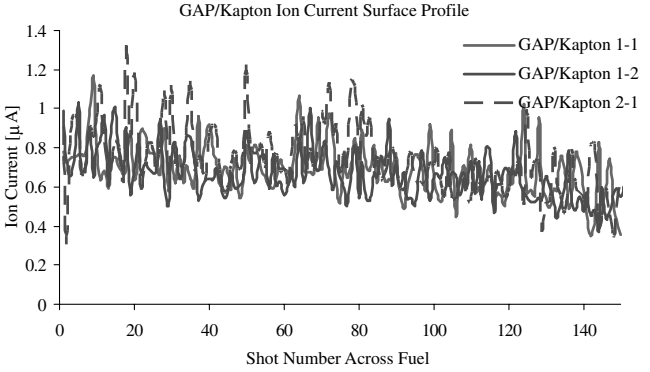

Fig. 14 GAP/Kapton average ion currents.

4.5×10^{7} cm^{-3} while the calculated average ionization fraction is 8.2×10^{-8}. Although the downstream location of the peak ion currents is the same for both GAP cases, the greater peak ion currents are again consistent with the smaller thickness GAP backed with Kapton.

The peak ion currents were again measured over 150 shots across 2.5 cm of the fuel. This result is illustrated in Fig. 14. The peak values of the average ion currents for the Kapton-backed GAP are shown to be significantly higher than when the GAP is backed with acetate. This is again attributed to the thickness of the target material. When there is less material, more of the laser energy can be transmitted through the substrate and subsequently directed toward ionization, as evident with the higher ion density and ionization fraction for the Kapton-backed as opposed to the acetate-backed GAP. The resulting lower ion densities and ionization fractions from the GAP/acetate are due to more of the deposited laser energy going into heating the thicker material as opposed to ionizing the thinner GAP/Kapton.

C. PVC/Acetate

Of the two target materials, PVC and GAP, the PVC appears to exhibit more favorable performance characteristics. The PVC strip tested here was $\sim$45 μm thick with 115 μm acetate backing (Figs. 15a and 15b). The thickness of the PVC is now half of the GAP/Kapton and reduced by a factor of 6 over the GAP/acetate. Similar test conditions to the GAP were applied to the PVC testing where 24.5 mJ were deposited over 5 ms. However, the volume of mass ejected was 2.5×10^{-7} cm^3 corresponding to 3.4×10^{-7} g/shot or 0.34 mg/shot of PVC ejected. The amount of PVC mass ejected is obviously much lower than either GAP case based on the reduced thickness of the PVC.

Of the different fuel/substrate combinations, the PVC/acetate had the highest average ion density of 7.9×10^{9} cm^{-3} and an estimated ionization fraction of 5.1×10^{-7} at 6 cm from the target face. This was the downstream location where the greatest peak ion current was measured. To find this location, the ion current was measured at incremental distances downstream. This is illustrated in Fig. 16.

Figure 16 shows the current initially starts out small at 0.8 μA at 3 cm in front of the PVC and then rapidly expands to a peak value of 1.2 μA at 6 cm. This expansion is observed to take place within 100 μs.

In addition to seeing how the peak currents vary with the downstream location, it is also of interest to see the effect of how the ion current changes by increasing the amount of deposited energy. Figure 17 shows the results of measuring the average ion current at increasing energy levels. The ion currents of the four measured energy levels are taken at 6 cm. This location was selected because it was found from Fig. 16 to be the downstream location where the peak ion current occurs. By increasing the amount of energy deposited into the same amount of mass, Fig. 17 illustrates how greater ion currents can be achieved as a result of increasing the kinetic temperature through greater incident energy.

A summary of the calculated results for each target material and substrate combination is shown in Table 2. It should be pointed out

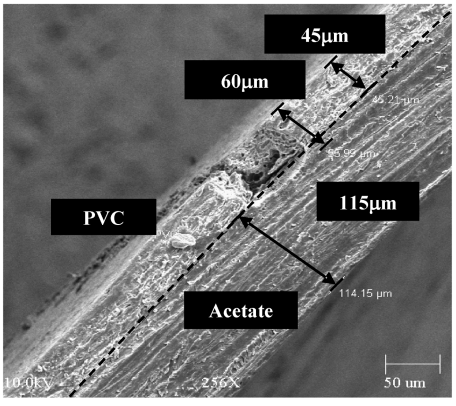

a)

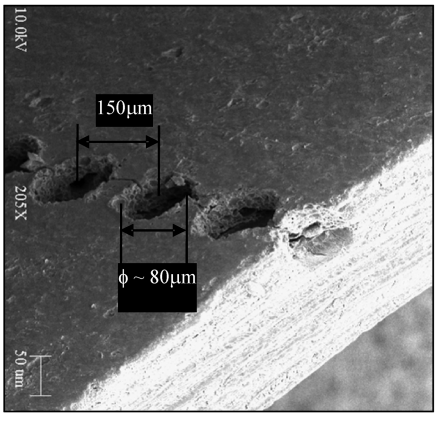

b)

Fig. 15 a) PVC/acetate SEM photo; b) PVC/acetate SEM photo.

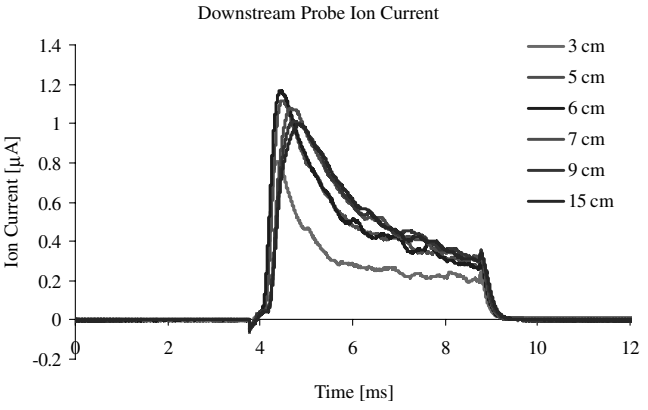

Fig. 16 Downstream probe ion currents.

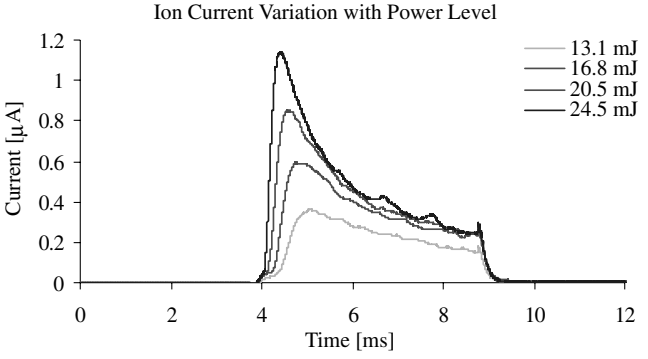

Fig. 17 Ion current variation with increasing power.

Table 2 Summary of calculated results for each target/substrate

Fuel	Substrate	μg/shot	n_{ion}, cm^{-3}	f (ionization fraction)
GAP	Acetate	5.10	1.60E + 07	9.80E − 09
GAP	Kapton	1.70	4.50E + 07	8.20E − 08
PVC	Acetate	0.34	7.90E + 09	5.10E − 07

that the lower ablated mass samples correspond to a higher ionization fraction. This is a consequence of the fuel thickness in each case. The PVC being the thinnest of all three targets results in the highest ionization fraction because it has the highest energy per mass available to ionize the target with the same energy being used in each case.

V. Conclusions

Average ion currents and average ion densities have been measured on a μLPT using a negatively biased flat probe. These measurements were made for 24.5 mJ of energy deposited over a 5 ms discharge time for GAP and PVC materials. The results of these measurements show a very low ionization fraction in both PVC and GAP materials regardless of the substrate material that is backing them. One source of the low average ion currents and densities can be attributed to the relatively long discharge time of the μLPT. If this discharge time were to be shortened to the microsecond or nanosecond length while maintaining the same amount of energy deposited to the target, a rise in the ionization levels should be expected. Additionally, it should be pointed out that a conservative estimate for A_c was taken which may lead to the underestimation of the ion density. However, because at least 150 shots were taken before measuring the collection area, there is a reasonable confidence that this area was sufficiently characterized. Future work should include using a Langmuir probe with a well-known collection area to verify the densities calculated here. An additional method to increase the ionization level and in turn the I_{sp} of this propulsion device would be to optimize the fuel thickness. Measured ion currents indicate that a greater ionization is achieved in target materials that are incrementally thinner. This was evident as the peak ion current and the ionization fraction progressively increased from being low in the 300-μm thick GAP to reaching the maximum for the 55-μm thick PVC.

The peak ion currents measured at 150 successive locations over a 2.5 cm distance on a single fuel strip have also been measured. The results show how a material such as GAP can have very different ion currents between transverse locations. This is an indication that a higher ion current implies a smaller thickness at the respective target location. This would be because more laser energy is available for ionization rather than heating or neutral particle ejection.

Finally, the peak ion currents have been measured for PVC by increasing the amount of deposited laser energy. The more laser energy that is available for the same amount of PVC mass results in a greater number of particles being ionized. This result is consistent with those observed in the GAP material that as the thickness of the material is reduced, greater levels of ionization are achieved. The SEM analysis confirms this result by showing equal ablation crater diameters for GAP when two different GAP thicknesses were considered. In both cases, the GAP ablation diameter was the same; however, the thicker GAP (300 μm) resulted in a lower peak ion current and ionization fraction than the thinner GAP (115 μm).

Acknowledgments

This work was funded by the U.S. Air Force Research Laboratory, Electric Propulsion Laboratory. We would like to thank Claude Phipps of Photonics Associates and Jim Luke of New Mexico Engineering Research Institute for providing the propulsion unit. Additionally, we would like to thank Wes Helgeson of Mew Mexico Engineering Research Institute for manufacturing multiple target/substrate combinations. Special thanks go to Marietta Herndandez for providing images of the target and substrate materials from performing SEM measurements.

References

[1] Phipps, C. R., and Luke, J. R., "Diode Laser-Driven Microthrusters: A New Departure for Micropropulsion," *AIAA Journal*, Vol. 40, No. 2, 2002, pp. 310–318.

[2] Phipps, C. R., Luke, J. R., McDuff, G. G., and Lippert, T., "Laser Ablation Powered Mini-Thruster," *High Power Laser Ablation IV*, edited by Claude R. Phipps, SPIE Proceedings Vol. 4760, SPIE–International Society for Optical Engineering, Bellingham, WA, 2002, pp. 833–842.

[3] Singh, R. K., "Fundamental Processes During Laser Deposition of Thin Films," SPIE Proceedings Vol. 2045, SPIE–International Society for Optical Engineering, Bellingham, WA, 1994, pp. 10-27.

[4] Kelly, R., and Dreyfus, R. W., "Reconsidering the Mechanisms of Laser Sputtering with Knudsen-Layer Formation Taken into Account," *Nuclear Instruments and Methods in Physics Research Section B*, Vol. 32, Nos. 1–4, 1988, pp. 341–348. doi:10.1016/0168-583X(88)90235-2

[5] Casavola, A., Colonna, G., and Capitelli, M., "Non-Equilibrium Conditions During a Laser Induced Plasma Expansion," *Applied Surface Science*, Vol. 208–209, 2003, pp. 85–89. doi:10.1016/S0169-4332(02)01340-5

[6] Keidar, M., Boyd, I., Luke, J., and Phipps, C., "Plasma Generation and Plume Expansion for a Transmission-Mode Micro-Laser Ablation Plasma Thruster," AIAA 2003-4567, 2003.

[7] Boyd, I. M., and Keidar, M., "Simulation of the Plume Generated by a Micro Laser-Ablation Plasma Thruster," *High Power Laser Ablation IV*, SPIE Proceedings Vol. 4760, SPIE–International Society for Optical Engineering, Bellingham, WA, 2002, p. 852.

[8] Phipps, C. and Dreyfus, R., "Laser Ablation and Plasma Formation," *Laser Ionization Mass Analysis*, edited by A. Vertes, R. Gijbels, and F. Adams, Wiley, New York, 1993.

[9] Jones, F. L., and Willott, W. H., "Secondary Emission from Copper due to Slow Positive Ions of Argon," *Proceedings of the Physical Society, London*, Vol. 48, No. 6, 1936, pp. 830–838. doi:10.1088/0959-5309/48/6/302

[10] Kubota, N., and Aoki, I., "Burning Rate Characterization of GAP/HMX Energetic Composite Materials," *Propellants, Explosives, Pyrotechnics*, Vol. 25, 2000, pp. 168–171. doi:10.1002/1521-4087(200009)25:4<168::AID-PRE-P168>3.0.CO;2-B

[11] Halliday, D., Resnick, R., and Walker, J., *Fundamentals of Physics*, 7th ed., Wiley, New York, 2004, Chaps. 21,22.

[12] Photonics, "Fiber Optics: Understanding the Basics," *Photonics Design and Applications Handbook*, 2002, pp. H154–H157.

A. Gallimore
Associate Editor